RESEARCH ARTICLE | MARCH 13 2023

Improving the cooldown times for next-generation cryocooled gravitational-wave interferometers @ @ 🕬

Special Collection: Gravitational Wave Detectors

Edgard Bonilla : Jaimi Salone; Brian Lantz; ... et. al



Appl. Phys. Lett. 122, 114102 (2023) https://doi.org/10.1063/5.0143940





CrossMark

Articles You May Be Interested In

MODELING AND EXPERIMENTS ON FAST COOLDOWN OF A 120 Hz PULSE TUBE CRYOCOOLER

AIP Conference Proceedings (March 2008)

GENERAL METHOD FOR ESTIMATING COOLDOWN TIME

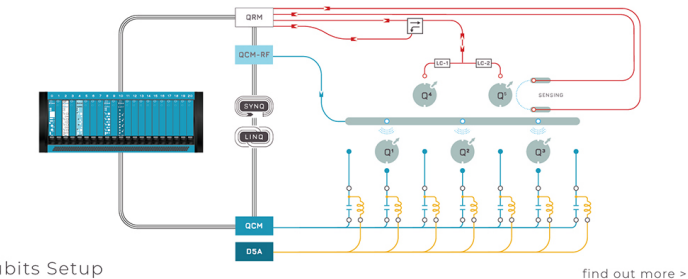
AIP Conference Proceedings (April 2010)

120 Hz pulse tube cryocooler for fast cooldown to 50 K

Appl. Phys. Lett. (February 2007)



Superconducting Qubits NV-Centers Spin Qubits



Spin Qubits Setup



Improving the cooldown times for next-generation cryocooled gravitational-wave interferometers () (s)

Cite as: Appl. Phys. Lett. **122**, 114102 (2023); doi: 10.1063/5.0143940 Submitted: 27 January 2023 · Accepted: 19 February 2023 · Published Online: 13 March 2023







Edgard Bonilla, 1,a) (D) Jaimi Salone, 1 Brian Lantz, 1 (D) Aaron Galper, 2 and Faith Stults 3

AFFILIATIONS

- Stanford University, Stanford, California 94305, USA
- ²Harvey Mudd College, Claremont, California 91711, USA
- ³Valley Christian Schools, San Jose, California 95111, USA

Note: This paper is part of the APL Special Collection on Gravitational Wave Detectors.

^{a)}Author to whom correspondence should be addressed: edgard@stanford.edu

ABSTRACT

We propose and test an exchange gas technique for improving the cooldown times of cryocooled gravitational-wave interferometers. The technique works by utilizing low-pressure dry nitrogen gas to create a path for heat conduction to test masses while protecting the rest of the in-vacuum equipment from unwanted heat leakage. We show that the technique is capable of shortening the total wait time to reach the operating temperature by a factor of 3.5. Additionally, our tests show that the improvement in the heat transfer rate can be predicted to be within 10% error by using the Sherman-Lees interpolation equation. The technique is compatible with vibration isolation requirements of the cryogenic shielding of 124 K silicon interferometers and has the potential to improve the iteration time for research and development. The scalability of the prototype, the ability to predict the heat conduction, and the simplicity of the engineering make the strategy a good candidate to be included in the cryogenic design of future cryocooled gravitational-wave interferometers. The findings mark a first step in the investigation for a strategy to mitigate ice formation on the interferometer optics during initial cooldown.

Published under an exclusive license by AIP Publishing. https://doi.org/10.1063/5.0143940

The first direct detection of gravitational waves by the Advanced LIGO Observatories in 2015¹ inaugurated the field of gravitational-wave astronomy, paving the way for exciting astrophysical discovery. To date, the LIGO and Virgo observatories have 90 astrophysical observations² with more expected in the future. Despite these exciting discoveries, much of the observable universe is still out of reach of current gravitational-wave antennas.³

The efforts to improve the existing technology are distributed in many areas, including in the design of next-generation terrestrial^{3–6} and extraterrestrial^{7,8} detectors and a maximization of detection capabilities of the existing infrastructure.^{9–11} The aim of these improvements is to extend the detection-frequency band and increase the uptime (or duty cycle) and sensitivity of the network of gravitational-wave detectors. The avenue for improvement we discuss here is operation at cryogenic temperatures by using silicon test masses at 124 K. This design choice is shared by LIGO Voyager,¹⁰ the second stage of Cosmic Explorer (CE2),³ and the Nuclear Matter Extreme Observatory (NEMO),⁵ and it has a series of potential benefits.¹²

First, the low operating temperature reduces the Brownian thermal noise from the optical coatings. Second, the high thermal conductivity of silicon enables operation at higher circulating optical power compared to current observatories, 13 reducing shot noise. Finally, silicon's thermal expansion coefficient crosses zero around 124 K, 14 leading to a drastic reduction in the thermoelastic noise. 10

Operating at 124 K enables the use of radiative cooling to maintain the temperature of the test masses. Radiation-only cooling is advantageous from a vibration isolation perspective because the closest mechanical connection between the test masses and the cooling equipment is the ground. A disadvantage of radiative cooling, however, is that the rate of heat transfer decreases significantly as the temperature of the optic decreases due to the T^4 dependence of radiation coupling. To increase the uptime of the observatories, we must minimize the impact of the cooldown time on operation. Two issues complicate the picture: ice formation on the optical surfaces and the large thermal mass of the test masses.

Deposition of water vapor on the surfaces of the optics at low temperatures can have a deleterious effect on the performance of the interferometer. Estimates suggest that under the ultimate vacuum conditions in Advanced LIGO, for a test mass at 124 K, an ice layer will grow at a rate of around 5 nm per day on the surface of the cooled optics. One way to avoid ice formation is to start lowering the

temperature of the optics only after the water vapor partial pressure is low enough to avoid ice deposition.

However, even when considering the geometry of the cryoshields and their cryotrapping effect, the vacuum quality needed to ensure that no ice grows on the surface of the test mass is only reached after the ion pumps are engaged, 17 days after closing the vacuum chamber in Advanced LIGO.18

On the other hand, the heavier proposed test masses (200 kg for LIGO Voyager¹⁰ for example) result in an increased heat capacity, pushing the expected radiation-only cooldown time to the order of

One proposed solution to this challenge is to supplement the cryoshield array proposed in Ref. 21 with a fast cooldown strategy. Faster initial cooldown would allow more flexible control of the temperature of the test masses, which can be quickly cooled when desired. This flexibility could then be used as part of a mitigation strategy for the ice buildup. For example, the test masses could be held at a higher temperature with an auxiliary heating system while the cryogenic shields are cold, preventing ice buildup until the water vapor pressure is low enough to be safe for the optics. This article is devoted to the exploration of a fast cooldown strategy based on exchange gas in an approach similar to the gas-gap heat switches in the cryogenics literature.²²⁻²⁴ We start by providing an overview of the theory of heat conduction through gases and conclude with a prototype to validate the

Heat conduction through a gas happens as the gas molecules interact with various surfaces, carrying energy between them. Depending on the frequency of intermolecular collisions, there are two extreme regimes of heat transfer: the free molecular flow and continuum regimes. The regimes are identified by using the Knudsen number, ²⁵ which is the ratio of the mean free path λ of the particles and the typical separation lengthscale L,

$$Kn = \frac{\lambda}{L}.$$
 (1)

The free-molecular flow regime occurs when $Kn \gg 1$ (typically $Kn \gtrsim 10$).²⁶ Heat conduction happens mostly by direct interactions between single particles and the walls, implying a linear relation between heat transfer and pressure.

Under the assumption of steady state flow of particles from either surface, the free-molecular heat transfer rate q''_{FM} is found to be²⁶

$$q_{FM}'' = -\alpha \sqrt{\frac{8k_B}{\pi m}} \left(1 + \frac{\zeta}{4}\right) P\left(\sqrt{T_h} - \sqrt{T_c}\right),\tag{2}$$

where *P* is the gas pressure, ζ is the number of internal degrees of freedom of each gas particle, and m is the particle's mass. T_h and T_c represent the temperatures of a hot and cold surface, respectively. $0 < \alpha < 1$ is the accommodation coefficient, which is a measure of the elasticity of the collisions between the particles and the walls. A value of $\alpha = 1$ implies that collisions are completely inelastic, and the particles thermalize with both surfaces on collision.

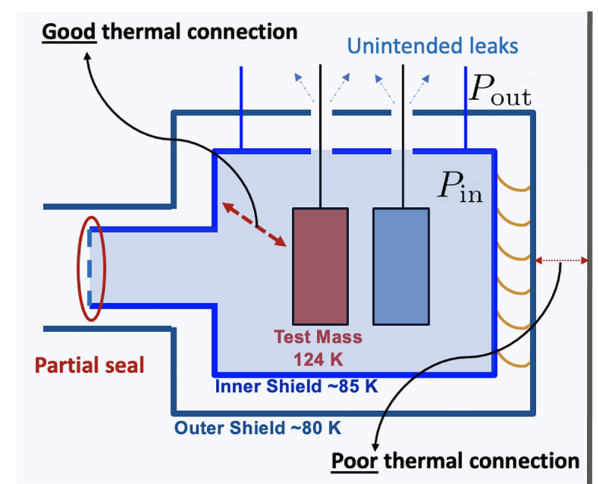
The other extreme for heat transfer is the continuum regime, occurring when $Kn \lesssim 10^{-2}.^{26,30}$ The heat transfer happens through a diffusion process similar to any other continuum medium. The prevalence of intermolecular collisions implies the heat transfer is roughly constant with pressure in this regime. Let $k_g(T)$ be the temperaturedependent, but pressure independent, thermal conductivity of the gas, and let L be the separation between two surfaces. The heat flux from the hot surface is given by

$$q_C'' = -\frac{1}{L} \int_{T_-}^{T_h} k_g(T) dT.$$
 (3)

As we explore later, the ideal operating conditions for the fast cooldown strategy lie in the transition regime between the two extremes, where $Kn \approx 1$. In the transition regime, the assumptions used to derive the previous equations break down, and it becomes challenging to provide a closed form expression for the heat flux.² Nevertheless, there is a semi-empirical equation that has been validated experimentally for a variety of gases 31,32 and is known to reproduce the results of various experiments to within 10% deviation.³³ The conductive heat flux between two surfaces through a gas in the transition regime is approximately given by the Sherman-Lees interpolation equation,

$$\frac{1}{q_T''} = \frac{1}{q_C''} + \frac{1}{q_{FM}''},\tag{4}$$

where $q_{FM}^{\prime\prime}$ and $q_C^{\prime\prime}$ are given in Eqs. (2) and (3), respectively. The exchange gas fast cooldown strategy is depicted in Fig. 1. The interior of the radiation shield is held at locally higher pressure $P_{\rm in}$ by injecting a suitable exchange gas. This increases the thermal conductivity to the optics enclosed. However, the benefit of increased heat transfer must be balanced with protecting the environment outside the cold shields from unwanted heat conduction. This can be solved by creating a pressure differential between the environment surrounding the test mass and the one outside the cryoshields despite unintended leaks, as depicted in Fig. 1. A pressure $P_{\text{out}} \ll P_{\text{in}}$ to the vacuum chamber ensures that the equipment outside of the cryoshields can remain at room temperature. A reasonable target is to hold the outside pressure Pout about two orders of magnitude lower than



Vacuum wall and Other components ~300K

FIG. 1. General approach of the exchange gas fast cooldown. A pressure differential is maintained to improve heat conduction inside the inner shield but poor conduction to the vacuum wall and other room-temperature components. A partial seal must be applied to the cryoshields to minimize unwanted gas leakage.

 $P_{\rm in}$. This ensures that there will be negligible heat conduction between the cold shields and the rest of the devices in the vacuum chamber.³⁴

Figure 2 shows a simplified plot for the heat flux between two plates at fixed separation L with varying pressure. The ideal choice for operating pressure for the exchange gas heat transfer scheme lies in the transition regime, when $\mathrm{Kn} \approx 1$. Adding more gas pressure to the vicinity of the test mass will have negligible impact on the heat transfer but will increase the amount of gas leaking into the main vacuum volume, increasing the risk of unwanted heat conduction to the room temperature equipment.

In terms of the specific exchange gas, we must select a readily available, high purity gas that can be easily pumped out of the vacuum chamber once the initial cooldown is over and will not compromise the functioning of any component of the vacuum system. We believe that molecular nitrogen (N_2) and helium (He) are the best candidates for the strategy. Between them, we chose molecular nitrogen (N_2) as the exchange gas for the cooldown strategy after analyzing tradeoffs among heat transfer, availability, and compatibility with vacuum requirements.

While helium has a higher heat transfer coefficient than nitrogen in the continuum regime (7.5 times higher at 100 K³⁰) in the free-molecular flow regime, its low accommodation coefficient (on the order of 0.3^{25,35} vs nitrogen's 1²⁵) almost completely invalidates its advantage over nitrogen. Additionally, a practical matter of concern is that helium is commonly used for leak detection devices in vacuum systems, which decreases its appeal as a choice for exchange gas. Finally, since nitrogen is likely to be used as the primary coolant for 124 K cryocooled detectors, there will be a source of high-purity nitrogen readily available to be used as exchange gas. Nevertheless, there is still room for discussion about the potential benefits of using a different exchange gas both for future prototype facilities as well as the full-scale observatories.³⁶

To demonstrate the feasibility of using nitrogen as the exchange gas, we must showcase a mechanism for feeding nitrogen into the interior of the inner shield and hold a pressure differential like the one in Fig. 1 despite an engineered leak to the main vacuum volume. To this

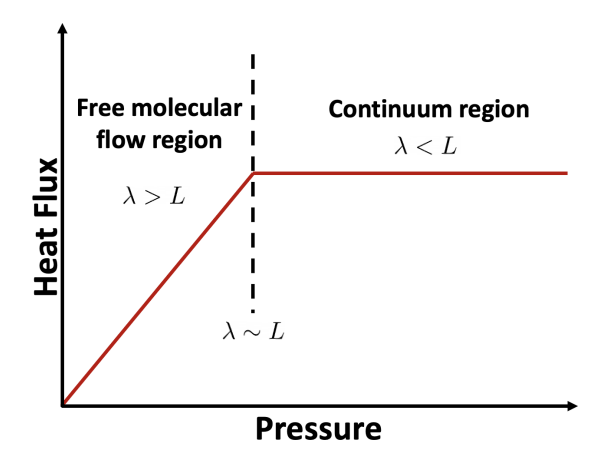


FIG. 2. Simplified plot of gas-mediated heat flux vs gas pressure across multiple orders of magnitude with other variables fixed. The heat flux increases with increasing pressure but becomes approximately constant once the continuum regime is reached. The goal of the fast cooldown strategy is to operate in the transition region $\lambda/L \approx 1$.

end, we will observe the cooldown curves for a 1-kg, 6-in. in diameter cylindrical silicon mass separated by a distance of 1 mm from the inner cryoshield surface by spherical glass beads under multiple exchange gas conditions. To achieve Kn \approx 1, we calculate the pressure such that the mean-free-path $\lambda \approx$ 1 mm for the range of operating temperatures using the equation for the mean free path, 37

$$P = \frac{\mu}{\lambda} \sqrt{\frac{\pi k_{\rm B} T}{2m_{N_2}}},\tag{5}$$

where μ is the (temperature-dependent) dynamic viscosity of nitrogen, 30 m_{N_2} is the mass of a nitrogen molecule, and $k_{\rm B}$ is Boltzmann's constant. For the temperature range of 300–100 K, this yields a range for the operating pressure:

$$10 \,\mathrm{mTorr} \le P_{\mathrm{in}} \le 50 \,\mathrm{mTorr}.$$
 (6)

We select the nominal operating pressure to be $P_{\rm in}=30\,{\rm mTorr}$, right in the middle of this range. The pressure of the rest of the vacuum chamber is expected to stay in the range of $P_{\rm out}\sim 10^{-4}\,{\rm Torr}$. We monitor the pressure inside the inner shield with a hot filament pressure gauge, accurate down to 1 mTorr. The pressure in the main vacuum is monitored by a cold cathode gauge.

To achieve the pressure differential, we re-purpose the prototype dual cryoshields from Ref. 21 to add a gas feedthrough. We include a small turbopump connected to the outside of the outer shield to help remove the excess exchange gas. We also create an artificial leak by leaving some of the access holes of the outer shield open, totaling around 1 cm² of opening to the main chamber.

The exchange gas feeding tube is connected to a nitrogen boiloff subsystem that releases the exchange gas into the cryoshields by utilizing choked flow,³⁸ so that the gas flow rate is dependent only on the upstream pressure. To attain the flow rate needed to hold the cryoshields at 30 mTorr by using a micrometer valve, the upstream pressure is estimated to be in the 10–50 Torr range. The vacuum connections for the exchange gas feeding subsystem are shown in Fig.

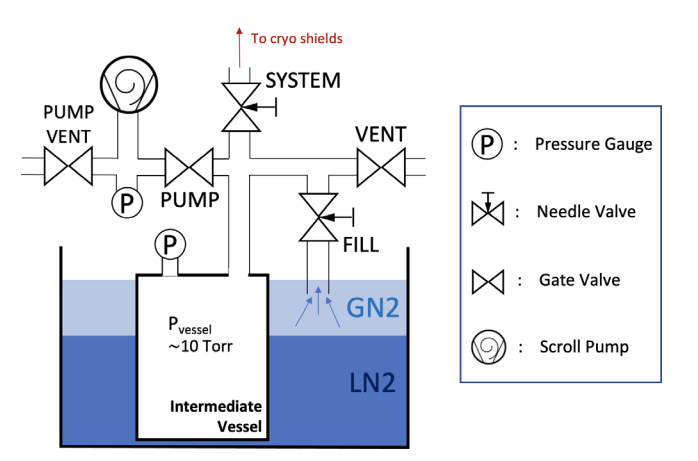


FIG. 3. Vacuum diagram for the exchange gas feedthrough subsystem. The intermediate vessel is filled with cold, low pressure boiloff nitrogen from a pool of liquid nitrogen it rests on. By setting the "SYSTEM" needle valve to a given position and manipulating the "FILL" valve, we can control the gas input to the cryoshields using choked flow.

3. The intermediate vessel is evacuated to a rough vacuum through the "PUMP" connection. Next, it is filled through the "FILL" port with cold, low pressure nitrogen boiloff from the liquid nitrogen pool it is sitting on (which serves the double function of keeping the gas inside the can at an acceptable temperature) up to the desired upstream pressure. At that point, we feed exchange gas to the shields by opening the "SYSTEM" valve. We control the pressure in the intermediate vessel by adjusting the "FILL" valve while we keep the "SYSTEM" valve at a set position, which controls the exchange gas flow rate to the cryoshields due to the properties of choked flow.

We set four temperature monitors in the system. They monitor the inner and outer shields, the silicon mass, and the seismic isolation table underneath the cryoshields. These temperature sensors allow us to determine the impact of the exchange gas on the cooldown time of the silicon mass, as well as the potential impact on nearby structures that need to be kept at room temperature.

To assess the cooldown curves quantitatively, we must separate the effects of radiative and exchange gas cooldown. We estimate the effective emissivity ε for the silicon mass inside the inner shield by performing a preliminary run with no exchange gas and fitting this radiation-only cooldown data to the Stefan–Boltzmann law,

$$mc_p(T)\frac{dT_{\rm Si}}{dt} = -A_{\rm total}\varepsilon\sigma(T_{\rm Si}^4 - T_{\rm inner}^4),$$
 (7)

where $T_{\rm Si}$ and $T_{\rm inner}$ are the silicon-mass and inner-shield temperatures, respectively. $\sigma=5.67\times10^{-8}\frac{\rm W}{\rm m^2K^4}$ is the Stefan-Boltzmann constant, $A_{\rm total}$ is the total surface area of the silicon optic of mass m, and $c_p(T)$ is the (temperature dependent) specific heat capacity of silicon, obtained from Ref. 39. We compute the numerical derivative of the observed data $\frac{dT_{\rm Si}}{dt}$ by using the total variation method described in Ref. 40. This analysis results in an effective emissivity $\varepsilon=0.75\pm0.02$ in agreement with similar measurements for silicon.

Figure 4 summarizes the effectiveness of the exchange gas on reducing the cooldown time. For the nominal 30 mTorr operating pressure, the time needed for the 1-kg silicon mass to reach 124 K was reduced to about 3 h from the initial 11 h of radiation-only cooldown.

We also note that adding more gas beyond the point where $Kn \approx 1$ has diminishing returns in terms of cooldown time, as expected from the sketch in Fig. 2. Our auxiliary sensors also verified that the seismic isolation table remains essentially at room temperature (changes observed are of less than $1\,K$ over several hours) under all exchange gas conditions.

The blue traces in the quadrants of Fig. 5 show the measured heat absorbed from the silicon mass as a function of time for different exchange gas settings. We estimate the heat transferred from the 1-kg silicon mass by the equation $|\frac{dE}{dt}| = mc_p(T)|\frac{dT_{\rm SI}}{dt}|$ using the numerical derivative of the temperature data. The specific heat of silicon as a function of temperature was obtained from Ref. 39.

In order to estimate the heat flow through gas conduction, we use the Sherman-Lees interpolation Eq. (4), which requires us to calculate the free-molecular and continuum regime heat fluxes,

$$q_{FM}^{"} = \alpha \sqrt{\frac{8k_B}{\pi m_{N_2}}} \left(1 + \frac{\zeta_{N_2}}{4}\right) P\left(\sqrt{T_{\text{in}}} - \sqrt{T_{\text{Si}}}\right),$$
 (8)

$$q_C'' = \frac{1}{L} \int_{T_{c_1}}^{T_{in}} k_g(T) dT.$$
 (9)

 $T_{\rm in}$ and $T_{\rm Si}$ represent the measured inner shield and test mass temperatures as a function of time, respectively. The accommodation coefficient can be taken to be $\alpha=1$ for most of the range of temperatures considered,²⁵ and the number of internal degrees of freedom for the nitrogen molecule is $\zeta_{N_2}=2.^{26}$ The mass of a nitrogen molecule is $m_{N_2}=4.65\times 10^{-26}$ kg. The thermal conductivity of gaseous nitrogen is modeled according to³⁰

$$k_g(T) = \frac{2.57 \times 10^{-3} \sqrt{T}}{1 + (235.5/T)(10^{-12/T})} [W/(m \cdot K)],$$
 (10)

where T is the temperature in kelvin. Finally, the inner shield pressure was measured and plugged directly into Eq. (8). Manual control of the pressure explains the fluctuations in heat transfer observed in Fig. 5.

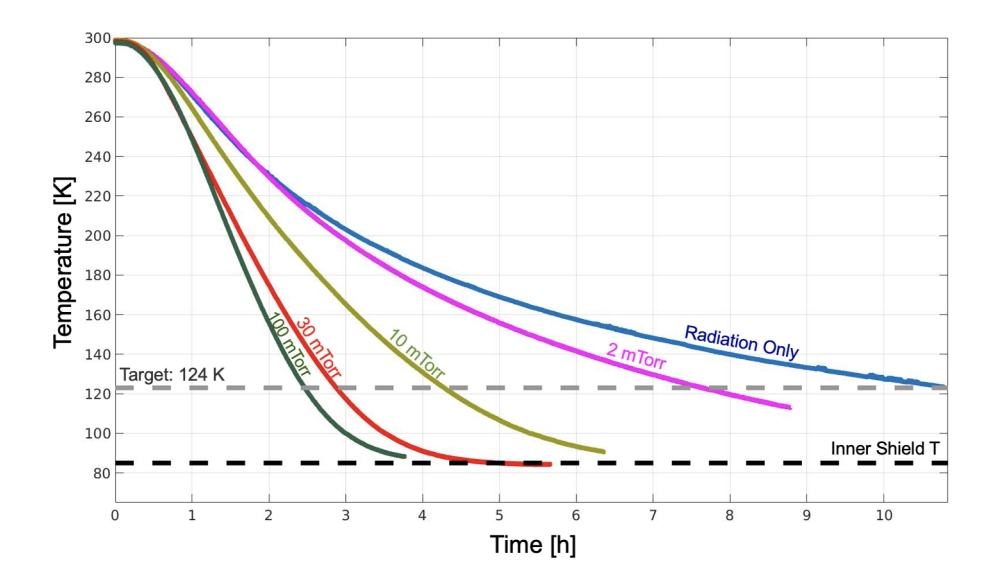


FIG. 4. Measured cooldown curves for the 1 kg mass under different exchange gas pressures inside the cryoshields. The nominal operating pressure of 30 mTorr achieves a cooling time 3.5 times shorter than the radiation-only condition. Further increasing the pressure inside the cryoshields has negligible impact on the cooldown times.

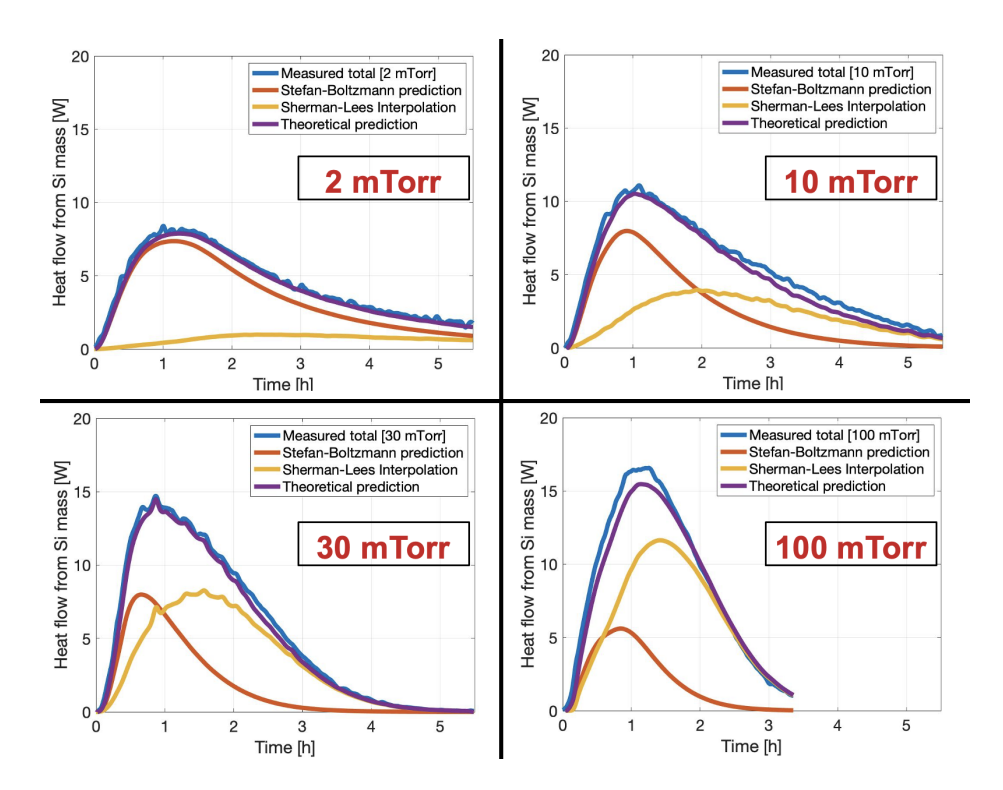


FIG. 5. Heat flow from the 1-kg silicon mass as a function of time for the different exchange gas cooldown experiments. The observed heat exchange is well fit by using a combination of radiation coupling and transition-regime gas conduction for the different pressures under consideration.

Figure 5 shows the results of the gas conduction analysis for the four different pressure settings. The total theoretical prediction (purple trace in Fig. 5) shows good agreement with the measured heat flux from the silicon mass for the pressure range studied. The expected theoretical contributions from radiation and conduction are shown in the red and yellow traces, respectively. It can be seen that gas conduction continues to contribute a significant fraction of the heat transfer late into the cooldown process, where radiation cooling is not effective anymore. We highlight that the theoretical prediction from the interpolation equation underestimates the actual heat flux. Agreement within 10% is consistent with other observations in the literature 33 but could also be due to having neglected convective heat transfer and heat conduction through the 1-mm spacers separating the silicon mass from the inner shield.

The results of our experiments show the potential of the exchange gas strategy for faster cooldown of cryocooled gravitational-wave interferometers. We show that with modest engineering, it is possible to create a mechanism to feed and control exchange gas flux into a vacuum chamber. With a 1 mm gap and 30 mTorr of nitrogen pressure, we were able to improve the radiation-only cooldown by a factor of 3.5.

Three reasons lead us to believe this strategy is viable for use in cryocooled gravitational wave detectors. First, the use of dry nitrogen as the exchange gas allows a return to normal vacuum operations within minutes of completing the initial cooldown in line with established knowledge of vacuum systems. This ensures that any time gained by faster cooldown is not offset by the time it takes to pump out the exchange gas.

The second reason is that the heat transferred by radiation and conduction through exchange gas both scale with the surface area of the mass, so we expect their relative contributions to be similar to what was observed in the prototypes.

The third reason is our ability to make theoretical estimates via the Sherman-Lees interpolation equation. The predictions enable the design of the initial cooldown cycle, which can be made to be fast and reliable and engineered to circumvent the ice buildup on the surface of the optics. Furthermore, the designs can be improved by adapting some of the current heat switch technologies (see Ref. 43 for some examples) to the specific needs of gravitational-wave detectors.

Beyond the horizon of the 124 K silicon technology, the ideas and techniques presented here can also be applied to improve the initial cooldown for other gravitational-wave detectors planning to use cryogenic temperatures such as the Einstein Telescope, provided a suitable selection of the exchange gas. ⁴⁴ The inclusion of fast cooldown strategies will shorten the iteration time for research and development of the technologies and practices needed to operate a cryocooled gravitational-wave observatory. Additionally, the flexibility granted by faster cooldown can be utilized as part of a mitigation strategy for the ice buildup on the surface of the optics, an endeavor that must be further explored in future work. We hope that this demonstration will inspire the inclusion of exchange gas as an integral part of the design of cryocooled gravitational-wave interferometers and their supporting research facilities.

The authors thank Kyle Godbey, Sina Köhlenbeck, Odylio Aguiar, and Pablo Giuliani for their feedback on this manuscript. This material is based upon the work supported by the National Science Foundation under Grant No. 2011786.

AUTHOR DECLARATIONS Conflict of Interest

The authors have no conflicts to disclose.

Author Contributions

Edgard Bonilla: Conceptualization (equal); Formal analysis (equal); Investigation (equal); Methodology (equal); Project administration (equal); Supervision (equal); Writing – original draft (equal); Writing – review & editing (equal). Jaimi Salone: Formal analysis (equal); Investigation (equal); Methodology (equal). Brian Lantz: Conceptualization (equal); Formal analysis (equal); Funding acquisition (equal); Investigation (equal); Methodology (equal); Project administration (equal); Visualization (equal); Writing – original draft (equal); Writing – review & editing (equal). Aaron Galper: Investigation (equal); Methodology (equal). Writing – original draft (equal). Faith Stults: Investigation (equal); Methodology (equal).

DATA AVAILABILITY

The data that support the findings of this study are available from the corresponding author upon reasonable request.

REFERENCES

- ¹B. P. Abbott, R. Abbott, T. Abbott, M. Abernathy, F. Acernese, K. Ackley, C. Adams, T. Adams, P. Addesso, R. Adhikari *et al.*, "Observation of gravitational waves from a binary black hole merger," Phys. Rev. Lett. **116**, 061102 (2016).
- ²The LIGO Scientific Collaboration, The Virgo Collaboration, The KAGRA Collaboration *et al.*, "GWTC-3: Compact binary coalescences observed by LIGO and Virgo during the second part of the third observing run," eprint arXiv:2111.03606 (2021).
- ³D. Reitze, R. X. Adhikari, S. Ballmer *et al.*, "Cosmic Explorer: The U.S. contribution to gravitational-wave astronomy beyond LIGO," https://baas.aas.org/pub/2020n7i035 (2019).
- ⁴M. Punturo, M. Abernathy, F. Acernese, B. Allen, N. Andersson, K. Arun, F. Barone, B. Barr, M. Barsuglia, M. Beker *et al.*, "The Einstein Telescope: A third-generation gravitational wave observatory," Class. Quantum Gravity 27, 194002 (2010).
- ⁵K. Ackley, V. Adya, P. Agrawal, P. Altin, G. Ashton, M. Bailes, E. Baltinas, A. Barbuio, D. Beniwal, C. Blair *et al.*, "Neutron star extreme matter observatory: A kilohertz-band gravitational-wave detector in the global network," Publ. Astron. Soc. Australia 37, e047 (2020).
- 6T. Akutsu and The KAGRA collaboration, "Large-scale cryogenic gravitational-wave telescope in Japan: KAGRA," J. Phys.: Conf. Ser. 610, 012016 (2015).
- ⁷J. Harms, F. Ambrosino, L. Angelini, V. Braito, M. Branchesi *et al.*, "Lunar gravitational-wave antenna," Astrophys. J. **910**, 1 (2021).
- 8K. Danzmann and LISA study Team, "LISA: Laser interferometer space antenna for gravitational wave measurements," Class. Quantum Gravity 13, A247–A250 (1996).
- ⁹J. Miller, L. Barsotti, S. Vitale, P. Fritschel, M. Evans, and D. Sigg, "Prospects for doubling the range of advanced LIGO," Phys. Rev. D 91, 062005 (2015).
- ¹⁰R. X. Adhikari, K. Arai, A. Brooks, C. Wipf, O. Aguiar, P. Altin, B. Barr, L. Barsotti, R. Bassiri, A. Bell *et al.*, "A cryogenic silicon interferometer for gravitational-wave detection," Class. Quantum Gravity 37, 165003 (2020).
- The Virgo Collaboration, "Advanced Virgo Plus phase I. Design report," Technical Report No. VIR-0596A-19 (2019), https://tds.virgo-gw.eu/?content=3&r=15777.
- ¹²KAGRA⁶ and the Einstein Telescope⁴ also work at cryogenic temperatures but much lower than 124 K. While the exchange gas technique in this article could prove useful in their context, the detailed implementation needs to be adapted to fit the specific constraints of those detectors.

- ¹³Higher thermal conductivity implies that the temperature of silicon optics will be more uniform than fused silica optics. Consequently, thermal distortions caused by absorbed laser power will be reduced in the silicon optics.
- 14.T. Middelmann, A. Walkov, G. Bartl, and R. Schödel, "Thermal expansion coefficient of single-crystal silicon from 7 K to 293 K," Phys. Rev. B 92, 174113 (2015)
- 15 As an example, consider the heat flux between two plates at 85 and 200 K. Even with unity emissivity, we expect about $90 \, \text{W/m}^2$ of radiative cooling, whereas conduction through a 1 mm gap of air can transport over $1000 \, \text{W/m}^2$.
- ¹⁶K. Hasegawa, T. Akutsu, N. Kimura, Y. Saito, T. Suzuki, T. Tomaru, A. Ueda, and S. Miyoki, "Molecular adsorbed layer formation on cooled mirrors and its impacts on cryogenic gravitational wave telescopes," Phys. Rev. D **99**, 022003 (2019).
- ¹⁷J. Steinlechner and I. W. Martin, "Thermal noise from icy mirrors in gravitational wave detectors," Phys. Rev. Res. 1, 013008 (2019).
- ¹⁸E. Bonilla, "Ice layer formation in vacuum environments," Technical Document No. T1900786 (LIGO, 2019).
- ¹⁹L. Spallino, M. Angelucci, A. Pasqualetti, K. Battes, C. Day, S. Grohmann, E. Majorana, F. Ricci, and R. Cimino, "Cryogenic vacuum considerations for future gravitational wave detectors," Phys. Rev. D 104, 062001 (2021).
- 20 Estimates for a 200 kg mass place the cooldown time anywhere between 3 and 7 days, depending on geometric details of the cryo shields.
- ²¹B. Shapiro, R. X. Adhikari, O. Aguiar, E. Bonilla, D. Fan, L. Gan, I. Gomez, S. Khandelwal, B. Lantz, T. MacDonald *et al.*, "Cryogenically cooled ultra low vibration silicon mirrors for gravitational wave observatories," Cryogenics 81, 83–92 (2017).
- ²²R. Bywaters and R. Griffin, "A gas-gap thermal switch for cryogenic applications," Cryogenics 13, 344–349 (1973).
- 23H-M. Chang and H.-J. Kim, "Development of a thermal switch for faster cooldown by two-stage cryocooler," Cryogenics 40, 769–777 (2000).
- ²⁴T. Poole, T. Foster, and A. Matthews, "Gas-gap heat switches with negative room temperature conductor separation and their application to ultra-low temperature platforms," Cryogenics 130, 103632 (2023).
- perature platforms," Cryogenics 130, 103632 (2023).

 25 T. Flynn, Cryogenic Engineering, Revised and Expanded (CRC Press, Boca Raton, 2004).
- ²⁶G. A. Bird, Molecular Gas Dynamics and the Direct Simulation of Gas Flows (Clarendon Press, Oxford, 1994).
- 27W. Trott, D. Rader, J. Castaneda, J. Torczynski, and M. Gallis, "Experimental measurements of thermal accommodation coefficients for microscale gas-phase heat transfer," in 39th AIAA Thermophysics Conference, 2007.
- 28 The original version of this equation is known as Knudsen's formula, as mentioned in Ref. 29, the correction factor for internal degrees of freedom is attributed to Bird,²⁷ and we used the succinct form given in Ref. 26.
- ²⁹E. H. Kennard, *Kinetic Theory of Gases* (McGraw-Hill, New York, 1938).
- ³⁰J. Jensen, R. G. Stewart, W. Tuttle, H. Brechna, and A. Prodell, *Brookhaven National Laboratory Selected Cryogenic Data Notebook: Section VI. Properties of Nitrogen* (Brookhaven National Laboratory, 1980).
- ³¹F. S. Sherman, "A survey of experimental results and methods for the transition regime of rarefied gas dynamics," in *Rarefied Gas Dynamics: Proceedings of the Third International Symposium on Rarefied Gas Dynamics*, edited by J. A. Laurmann (Academic Press, Cambridge, 1963), Vol. 2, pp. 228–260.
- ³²L. Lees, "Kinetic theory description of rarefied gas flow," J. Soc. Ind. Appl. Math. 13, 278–311 (1965).
- 33F. W. Burkholder, "Transition regime heat conduction of argon/hydrogen and xenon/hydrogen mixtures in a parabolic trough receiver," Ph.D. thesis (University of Colorado at Boulder, 2011).
- 34A factor of 100 less outer pressure translates into 100 times less heat conduction in the free-molecular flow regime when compared to the volume inside the inner shields.
- 35A. L. McFall, "The thermal accommodation coefficient of helium and argon on an amorphous silicon-dioxide surface," in *Rarefied Gas Dynamics, Parts I and II*, edited by S. S. Fisher (American Institute of Aeronautics and Astronautics, Reston, 1978).
- ³⁶For example, helium has been proposed as an exchange gas during steady-state operation of the Einstein Telescope. 44
- ³⁷W. G. Vincenti and C. H. Kruger, *Introduction to Physical Gas Dynamics* (Krieger Publisher Company, Malabar, FL, 1975).
- ³⁸j. N. Tilton, "Fluid and particle dynamics," in *Perry's Chemical Engineers' Handbook*, 7th ed., edited by R. H. Perry and D. W. Green (McGraw-Hill, New York, 1997), Chap. 6.

- ³⁹P. Flubacher, A. Leadbetter, and J. Morrison, "The heat capacity of pure silicon and germanium and properties of their vibrational frequency spectra," Philos. Mag. 4, 273–294 (1959).
- ⁴⁰R. Chartrand, "Numerical differentiation of noisy, nonsmooth data," ISRN Appl. Math. 2011, 164564.
- ⁴¹M. Constancio, Jr., R. X. Adhikari, O. D. Aguiar, K. Arai, A. Markowitz, M. A. Okada, and C. C. Wipf, "Silicon emissivity as a function of temperature," Int. J. Heat Mass Transfer 157, 119863 (2020).
- A. Berman, Vacuum Engineering Calculations, Formulas, and Solved Exercises
 (Academic Press, Cambridge, MA, 2012).
 S. Shu, J. A. Demko, and J. E. Fesmire, "Heat switch
- ⁴³Q. S. Shu, J. A. Demko, and J. E. Fesmire, "Heat switch technology for cryogenic thermal management," IOP Conf. Ser. 278, 012133 (2017).
- ⁴⁴C. Reinhardt, A. Franke, J. Schaffran, R. Schnabel, and A. Lindner, "Gas cooling of test masses for future gravitational-wave observatories," Class. Quantum Gravity 38, 185003 (2021).